Plutonium-238 observations as a test of modeled transport and surface deposition of meteoric smoke particles

S. S. Dhomse,[1] R. W. Saunders,[2] W. Tian,[3] M. P. Chipperfield,[1] and J. M. C. Plane[2]

Received 3 July 2013; revised 6 August 2013; accepted 7 August 2013; published 28 August 2013.

[1] There are large uncertainties in the transport and surface deposition of upper atmospheric particles used to construct climate proxies. Here we use a 3-D chemistry-climate model (CCM) to simulate the transport and deposition of plutonium-238 oxide nanoparticles formed after the ablation of a power unit in the upper stratosphere (~11°S) in 1964. The model reproduces both the observed hemispheric asymmetry and time scale of Pu-238 deposition. We then use the CCM to investigate the transport of meteoric smoke particles (MSPs) from the upper mesosphere. The strongest MSP deposition is predicted to occur at middle latitudes, providing a significant source of Fe fertilization to the Southern Ocean. The model also predicts substantially more deposition in Greenland than in Antarctica (by a factor of ~15, in agreement with ice core measurements), showing that climate proxy measurements from a limited number of sites must be interpreted with care. **Citation:** Dhomse, S. S., R. W. Saunders, W. Tian, M. P. Chipperfield, and J. M. C. Plane (2013), Plutonium-238 observations as a test of modeled transport and surface deposition of meteoric smoke particles, *Geophys. Res. Lett.*, *40*, 4454–4458, doi:10.1002/grl.50840.

1. Introduction

[2] This paper describes a study of the transport of meteoric smoke particles (MSPs) from the upper atmosphere and their deposition at the Earth's surface. These nanometer-sized particles form in the upper mesosphere from the condensation of vapor produced by meteoric ablation and probably have an Fe-Mg-SiO_4 composition [*Hervig et al*., 2009; *Saunders and Plane*, 2011]. A major reason for understanding how MSPs are transported through the atmosphere, and their deposition mechanisms in the troposphere, is to interpret the recent measurements of extraterrestrial elements, including Ir, Pt, and superparamagnetic Fe, that have accumulated in polar ice cores [*Gabrielli et al*., 2004; *Lanci and Kent*, 2006; *Lanci et al*., 2007]. The deposition flux of meteoric material is determined by measuring the concentration of one of these elements in an ice sample and using the snow accumulation rate to obtain the flux. In the case of Ir and Pt, these elements are highly enriched in cosmic dust compared with crustal dust [*Gabrielli et al*., 2004]. Superparamagnetic Fe occurs in Fe-rich particles (which are estimated to have radii between 3 and 9 nm) trapped in the ice [*Lanci et al*., 2012].

[3] Measurements in ice cores in central Greenland [*Gabrielli et al*., 2004; *Lanci and Kent*, 2006] and Vostok and EPICA-Dome C in the Eastern Antarctic highlands [*Lanci et al*., 2007, 2012] show that the deposition rate in Greenland is ~15 times higher than that at Vostok and EPICA. The fact that the snowfall rate in central Greenland is about 8 times greater than the Antarctic interior implies that wet deposition is a more important removal mechanism for MSPs than dry deposition [*Lanci et al*., 2012]. The Greenland estimate of the total input of interplanetary dust particles (IDPs) into the Earth's atmosphere is around 200 t d^{-1}. This is significantly higher than most estimates based on observations within the atmosphere, which are consistent with an input of less than 70 t d^{-1} [*Plane*, 2012].

[4] Another reason for studying the transport of small particles from the middle atmosphere to the surface is to interpret surface measurements of particles containing ^{10}Be, which are produced mainly in the stratosphere by nuclear interactions between galactic cosmic ray particles and N_2. Records of ^{10}Be in polar ice cores have been used to study past solar activity [e.g., *Pedro et al*., 2012]. However, the interpretation of the ^{10}Be data is hampered by uncertainties in the way ^{10}Be-containing particles are transported and scavenged from the atmosphere [*Heikkilae et al*., 2009]. This problem is analogous to that of MSPs, except that while ^{10}Be particles are produced in both the upper troposphere and stratosphere–which complicates modeling their residence time in the atmosphere–MSPs are only produced in the upper mesosphere.

[5] A good test for a model of transport and deposition would be provided by a transient input of nanometer-sized particles in the middle atmosphere, and this was provided by the injection of ^{238}Pu into the stratosphere after the failed launch of a satellite nearly half a century ago. On 21 April 1964, a U.S. Transit navigational satellite launched from Vandenberg Air Force Base in California (34°N, 120°W) failed to reach orbital velocity. The payload included a SNAP-9A radioisotope thermoelectric generator, containing 17 kCi (about 1 kg) of ^{238}Pu (half-life = 88 years), which reentered the atmosphere in the Southern Hemisphere (SH) around 11°S over the Indian Ocean. Based on subsequent stratospheric inventories, it was concluded that the SNAP-9A ablated completely during reentry (as designed) and that all of the ^{238}Pu vapor subsequently recondensed as PuO_2 nanoparticles [*Krey*, 1967; *Krey and Krajewski*, 1970].

[6] Initially, the ablation altitude was estimated to be around 46 km [*Krey*, 1967]. $^{238}PuO_2$ particles were collected by high-altitude balloons and later analyzed using radioautography. The particles displayed a lognormal size distribution with a size range between 5 and 58 nm and a modal

[1]School of Earth and Environment, University of Leeds, Leeds, UK.
[2]School of Chemistry, University of Leeds, Leeds, UK.
[3]College of Atmospheric Sciences, Lanzhou University, Lanzhou, China.

Corresponding author: J. M. C. Plane, School of Chemistry, University of Leeds, Leeds LS2 9JT, UK. (j.m.c.plane@leeds.ac.uk)

0094-8276/13/10.1002/grl.50840

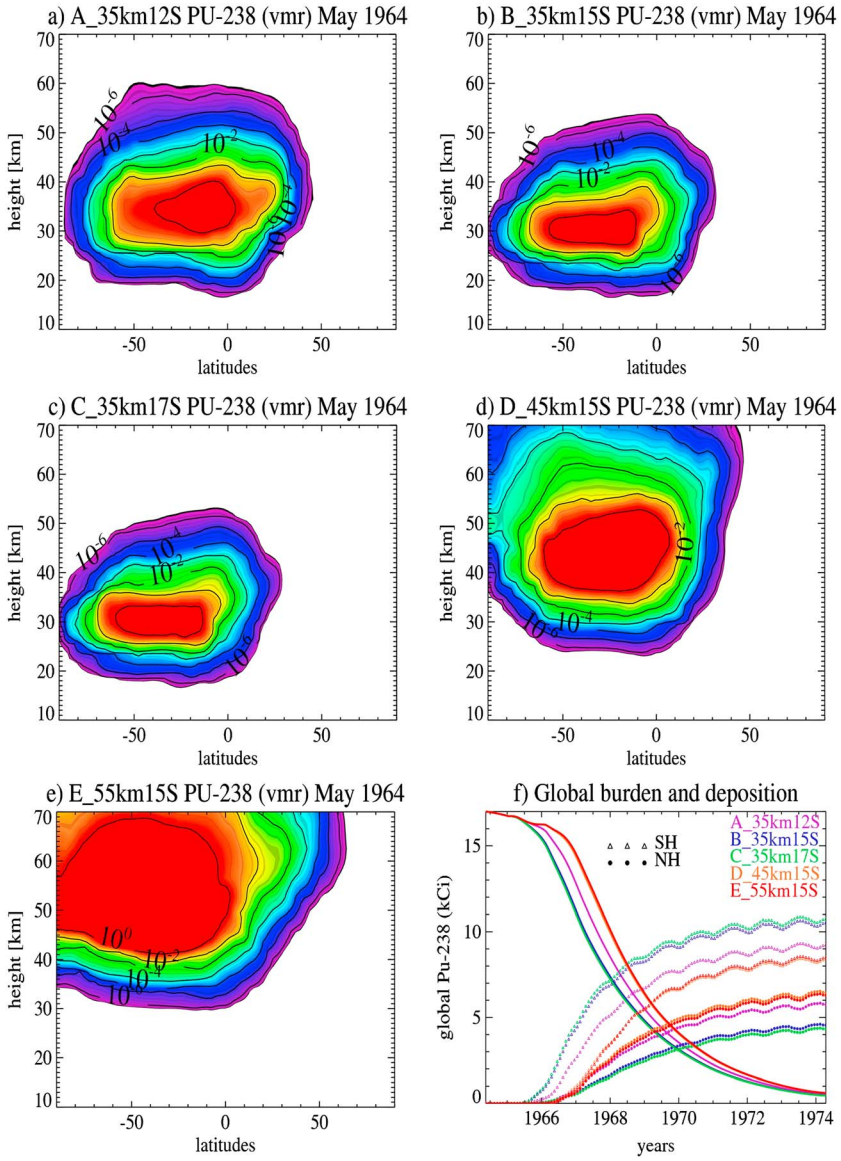

Figure 1. Modeled zonal mean mixing ratios of $^{238}PuO_2$ particles ($\times 10^{12}$ mol mol^{-1}) at the end of May 1964 (1 month after the injection) for five different model runs. Lower right panel: time series of global atmospheric burden of Pu-238 (solid lines in kCi) and deposited Pu-238 (in kCi) in SH (triangles) and NH (open circles) from five model runs.

mass of ~10^{-17} g [*Krey*, 1967]. Due to the uniqueness of the SNAP ^{238}Pu isotope (which differentiated it from atmospheric thermonuclear bomb tests), the spatial surface distribution of ^{238}Pu could be established from soil data at 65 sites (33 in the Northern Hemisphere (NH) and 32 in the SH) [*Hardy et al*., 1973]. The majority of the ^{238}Pu was observed in the SH, ~3.5 times more than that in the NH. Later reports of temporal surface deposition measurements from ice sheet surface layers and snowmelt indicated that the SNAP ^{238}Pu signal was first evident in south Greenland in 1966 [*Koide and Goldberg*, 1977] but significantly earlier (1964–1965) in Antarctica [*Cutter and Bruland*, 1979; *Koide et al*., 1979].

[7] For the present study, we use a 3-D global chemistry-climate model (CCM) to test the model's ability to reproduce the observed surface deposition of ^{238}Pu. Because of the uncertainty of the precise altitude and latitude at which the ablation occurred, these parameters were varied within reasonable limits in the model. The same CCM is then used to investigate transport of MSPs from the upper mesosphere to the surface and to convert the measured fluxes of Ir, Pt, and superparamagnetic Fe into estimates of the global IDP input rate. Section 2 of this paper describes the model and experimental setup, followed by results and discussion in section 3.

2. Model Description and Experiment Setup

[8] We have used the UMSLIMCAT 3-D Chemistry-Climate Model (CCM) to study the atmospheric transport and deposition of nanoparticles. The model is based on the UK Met Office Unified Model (v4.5) with a stratospheric chemistry scheme from the SLIMCAT model [*Tian and Chipperfield*, 2005]. The model has 64 vertical levels from the surface to 0.01 hPa (~80 km) and a horizontal resolution

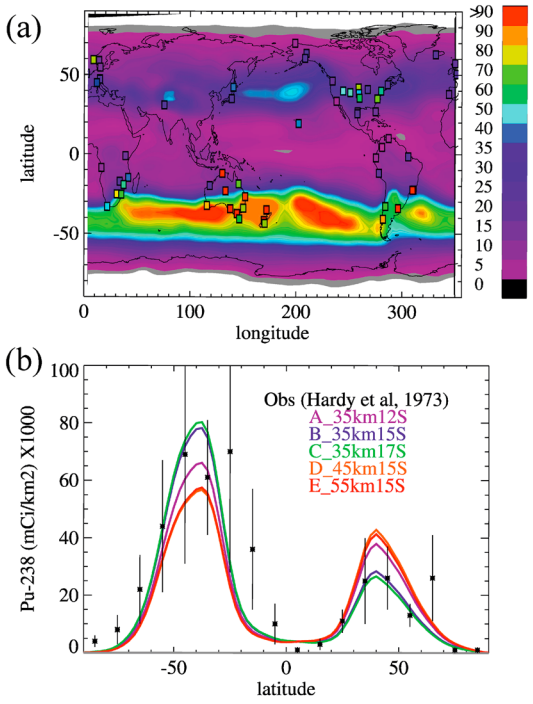

Figure 2. (a) Modeled deposition map (in mCi km^{-2}) from run B_35km15S. Measurement sites are indicated by the colored boxes; (b) Comparison of the zonal mean modeled deposition (in mCi km^{-2}) from the five model runs with observations [*Hardy et al.*, 1973, Tables 1 and 2].

of 2.5° × 3.75°. Model boundary conditions are similar to those used in the Chemistry-Climate Model Validation Activity for SPARC REF-2 simulation [*Morgenstern et al.*, 2010] but starting in May 1964. The model has generally performed well in recent stratospheric circulation tests [e.g., *Strahan et al.*, 2011].

[9] An inert tracer was added into the CCM to analyze the transport of $^{238}PuO_2$ particles resulting from the SNAP ablation. We assume that $^{238}PuO_2$ was converted exclusively to nanometer-sized particles [*Krey*, 1967], so that gravitational sedimentation below 50 km was negligible. The total number of particles injected at the location of the SNAP ablation in the stratosphere was scaled to 17 kCi of ^{238}Pu. These particles are removed in the model by dry deposition at the surface and wet deposition through the troposphere. There are large uncertainties in the rates of these processes and how to parameterize them as subgridscale processes in large-scale models [e.g., *Giannakopoulos et al.*, 1999]. Therefore, for both processes, we use a simplified approach, but one which allows us to model realistic magnitudes of $^{238}PuO_2$ particles (and MSPs) and investigate the factors that determine the observed hemispheric asymmetry in deposition. For dry deposition, the model assumes that 1% of the particles in the bottom model level (40 m deep) are removed every 30 min time step. This corresponds to a deposition velocity of 0.02 cm s^{-1} at the center of the model level. Initial experiments with dry deposition as the only $^{238}PuO_2$ removal process produced similar deposition in both hemispheres, which also occurred later than shown by observations (see section 1). MSP observations also suggest that wet deposition may be driving the observed differences in deposition between Greenland and Antarctica. The adopted wet deposition scheme is related to the occurrence of rain or snow in the model. When the relative humidity exceeds 100%, particles are removed with a lifetime of 0.72 h. This rate of scavenging, coupled with the occurrence of rain and snow, produces reasonable global deposition rates of $^{238}PuO_2$ particles (see below).

[10] After a 10 year spin-up, five 10 year runs (runs A–E) were initialized on 1 May 1964 with SNAP injection at different altitudes and latitudes (2.5° apart), which are designated as follows: A_35km12S means run A with ablation altitude of 35 km and latitude of 12.5°S at the center of the model grid; in runs B_35km15S and C_35km17S, ablation occurs at 35 km altitude and latitudes of 15°S and 17.5°S, respectively; and D_45km15S and E_55km15S have the same ablation latitude (15°S), but ablation occurs at 45 and 55 km, respectively. A sixth 20 year run (F) was initialized on 1 May 1964 with a constant 10 parts per trillion mixing ratio of 1.5 nm MSPs at the top model level (~80 km). This follows the procedure that we adopted recently for studying MSPs in the stratosphere [*Saunders et al.*, 2012].

3. Results and Discussion

[11] Figures 1a–1e show the zonal mean distribution of modeled $^{238}PuO_2$ particles, 1 month after the initialization, from the five model simulations. Although the specified SNAP ablation altitudes are identical in runs A_35km12S, B_35km15S, and C_35km17S, particles from run A_35km12S seem to have spread to most of the SH stratosphere, whereas particles from runs B_35km15S and C_35km17S are confined to the middle-lower stratosphere. The SNAP explosion corresponded to the time of year when the Brewer-Dobson (BD) circulation transport is toward the extratropical SH. Particle release in the deep tropics (12°S) experiences stronger upward motion in the ascending branch of the B-D circulation. Earlier estimates of the SNAP ablation altitude range from 46 to 60 km [e.g., *Hardy et al.*, 1973]. We performed two runs with a higher altitude injection of particles. In simulations D_45km15S and E_55km15S, the particles spread much more throughout the SH, because the particles were caught in the upper branch of the BD circulation and were transported to SH middle-high latitudes and higher altitudes. Some of these particles were also transported to the NH stratosphere via the strong (mesospheric) meridional circulation in summer. Middle stratospheric particles are transported to high latitudes via the descending branch of the BD circulation.

[12] As particles reach the lower stratosphere, they are mixed rapidly throughout low to middle latitudes by eddies that are generated by breaking planetary waves. Lower stratospheric particles are then transported to the troposphere via isentropic mixing [*Holton et al.*, 1995] and other processes such as tropospheric folds [*Appenzeller and Davies*, 1992]. However, at higher latitudes in the polar regions, the strongest stratosphere-troposphere exchange (STE) occurs in spring after vortex breakup [*Harris et al.*, 2008]. Figure 1f also shows the total accumulated particles in the SH and the NH from these five simulations. Observations indicated that ^{238}Pu first reached the surface in 1964 in the SH and in 1966 in the NH (see section 1). This timing seems to be reasonably well captured by the model. In particular, the earlier deposition from runs B_35km15S and C_35km17S appears to better fit the observations: 0.01% of the final ^{238}Pu deposition level is predicted in the SH at the end of

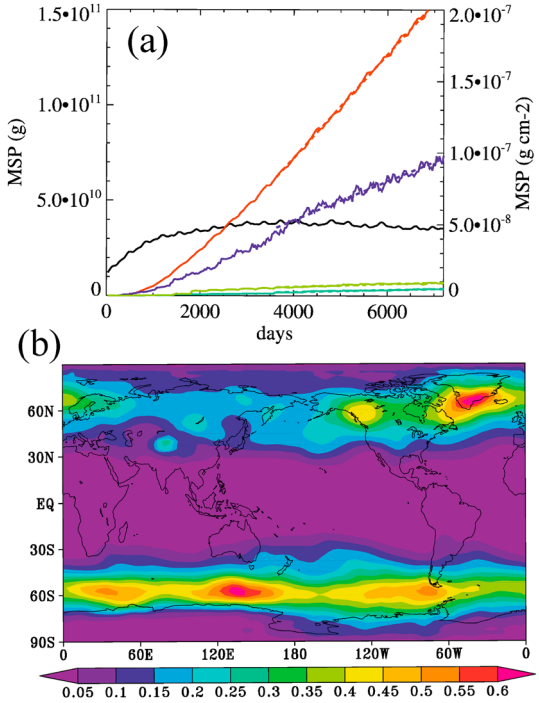

Figure 3. (a) Temporal evolution of total atmospheric mass burden of MSPs (black line) and the accumulated surface-deposited MSP mass (orange line), in g (left-hand ordinate). The deposition fluxes in g cm^{-2} d^{-1} (right-hand ordinate) are shown for GRIP (72°N, 38°W, blue line), VOSTOCK (78°S, 106°E, turquoise line), and DOME-C (75°S, 123°E, green line). The dashed lines are linear fits from the last 3650 days or 10 years. (b) Map of annual mean Fe deposition rates (in µmol Fe m^{-2} yr^{-1}) from run F_SMOKE.

1964, reaching 1% by mid-1965; in contrast, the 1% level is not achieved until spring 1966 in the NH. The model predicts a steady increase in the amount deposited until 1972 and shows that the atmospheric burden is essentially zero (<5% of original loading) by 1974.

[13] Figure 2a shows the modeled accumulated deposition from run B_35km15S by 1971 compared to observations. Overall, the model captures the asymmetry and overall magnitude of the total deposition by this date. However, the model does not predict the higher values at SH low latitudes (e.g., in North Australia). This discrepancy could be due to the direct sedimentation of larger particles. Note that the modeled deposition is sensitive to the injection location, which is highlighted in the zonal mean comparison shown in Figure 2b. If the injection is at higher altitudes (runs D_45km15S and E_55km15S), then more particles are transported and deposited in the NH. Similarly, if the injection is at lower latitudes, run A_35km12S, the particles are transported into the NH. From the model results, we can infer that the main SNAP release was near 35 km altitude and poleward of 12°S latitude.

[14] Given the satisfactory simulation of transport and deposition of ^{238}Pu from SNAP-9A, we then used the same model setup to investigate the deposition of MSPs from the upper mesosphere. Figure 3a shows the time series of the total atmospheric burden and accumulated deposition of MSPs at three polar locations. The MSPs in the model settle down to a steady state after about 6 years (2000 days), i.e., the atmospheric burden has stabilized at 3.7×10^{10} g (or 2×10^{30} particles), and the surface deposition is increasing linearly at 2.6×10^{7} g (or 1.4×10^{27} particles) per day. Note that the interannual variations in the BD circulation are much larger than the decadal changes, and the linear fits shown in Figure 3a have very small sigma values (less than 1%), so that these results should not be sensitive to the year in which the model is initialized. The mean residence time of particles in the atmosphere (burden/flux) is around 4.3 years. The deposition rate then balances the implied input flux at the top of the atmosphere with the fixed volume mixing ratio (vmr) boundary condition (vmr = 10 parts per trillion by volume at 80 km). Since the MSPs in the model have an assumed radius of 1.5 nm and a density of 2 g cm^{-3} [*Saunders et al.*, 2012], the equivalent global input of IDPs into the atmosphere is 26 t d^{-1}. This value, which is of course the ablated mass which recondenses to MSPs, was selected to be in accord with the range of estimates obtained from diverse measurements in the middle atmosphere [*Plane*, 2012].

[15] The model predicts that the deposition flux at the GRIP site in Greenland is 18 and 13 times larger than the fluxes at Vostok and EPICA Dome-C in central Antarctica, respectively. This is in good accord with the ice core flux measurements (see section 1), where the ratio of GRIP to Vostok/EPICA was about 15 [*Lanci et al.*, 2007]. The modeled flux at GRIP is 4.8×10^{-5} g m^{-2} yr^{-1}, which is a factor of 3.5 lower than the measured flux of 1.7×10^{-4} g m^{-2} yr^{-1}. For Vostok and EPICA, the measured fluxes are factors of 3.2 and 4.2 times higher, respectively. These results imply that the global input of 27 t d^{-1} used in the model is too low by a factor of 3–4, suggesting that the total ablated mass is between 75 and 100 t d^{-1}. Although this input rate is still consistent with several estimates using space-based techniques, it is too large by a factor of at least 2 to explain the metal atom layers in the mesosphere, optical extinction by MSPs, and the meteoric metal loading in the Junge sulfate layer [*Plane*, 2012].

[16] Figure 3b shows the predicted surface mass deposition flux over the Earth's surface. The strongest deposition occurs over northern and southern middle latitudes. The significant zonal asymmetry in the deposition arises from the geographical distribution of stratosphere-troposphere exchange. Deep exchange is driven by mountain ranges, as well as storm tracks over the North Atlantic, North Pacific, and, particularly, over the Southern Ocean between 50°S and 60°S. This is where the supply of bioavailable iron to phytoplankton is limited [*Johnson*, 2001]. The estimated input into the Southern Ocean from the model is ~0.4 µmol Fe m^{-2} yr^{-1}, which would scale up to around 1.5 µmol Fe m^{-2} yr^{-1} to be consistent with the deposition of superparamagnetic Fe at Vostok and EPICA (see above). This input should be compared with an Aeolian dust input of ~30 µmol Fe m^{-2} yr^{-1} [*Lancelot et al.*, 2009]. However, unlike continental mineral dust which has a low solubility (estimates vary from <1% to 10%), the MSP Fe should be in the form of highly soluble ferrous/ferric sulfate after processing in the stratospheric sulfate layer [*Saunders et al.*, 2012]. Thus, the input of bioavailable Fe from IDPs may be between 50% and 400% of the soluble Aeolian dust input. This could have significant climate implications because increased primary production will draw down CO_2 which is then exported to the deep ocean [*Smetacek et al.*, 2012].

4. Conclusions

[17] The measured deposition of $^{238}PuO_2$ particles in the years following the SNAP accident in 1964 is satisfactorily modeled using a simple wet deposition scheme in UMSLIMCAT. This agreement provides confidence in the modeled deposition pattern of MSPs, particularly since the deposition at high latitudes is consistent with ice core measurements of superparamagnetic Fe and Ir/Pt. However, a factor of 3–4 times larger meteoric ablation rate required to model the measured MSP flux, as opposed to the meteoric metal layers in the upper mesosphere, is a discrepancy which needs to be resolved in order to better quantify the deposition of bioavailable cosmic Fe to the Southern Ocean.

[18] **Acknowledgments.** This work was supported by the UK Natural Environment Research Council (grant NE/E005659/1). W. Tian is supported by the National Science Foundation of China (grants 41175042 and 41225018). We thank George Flynn (SUNY-Plattsburgh) for suggesting the use of SNAP data to test the CCM.

[19] The Editor thanks two anonymous reviewers for their assistance in evaluating this paper.

References

Appenzeller, C., and H. C. Davies (1992), Structure of stratospheric intrusions into the troposphere, *Nature*, *358*, 570–572.

Cutter, G. A., and K. W. Bruland (1979), Deposition and accumulation of plutonium isotopes in Antarctica, *Nature*, *279*, 628–629.

Gabrielli, P., et al. (2004), Meteoric smoke fallout over the Holocene epoch revealed by iridium and platinum in Greenland ice, *Nature*, *432*, 1011–1014.

Giannakopoulos, C., M. P. Chipperfield, K. S. Law, and J. A. Pyle (1999), Validation and intercomparison of wet and dry deposition schemes using Pb-210 in a global three-dimensional off-line chemical transport model, *J. Geophys. Res.*, *104*, 23,761–23,784.

Hardy, E. P., P. W. Krey, and H. L. Volchok (1973), Global inventory and distribution of fallout plutonium, *Nature*, *241*, 444–445.

Harris, N. R. P., et al. (2008), Ozone trends at northern mid- and high latitudes—A European perspective, *Ann. Geophys.*, *26*, 1207–1220.

Heikkilae, U., J. Beer, and J. Feichter (2009), Meridional transport and deposition of atmospheric Be-10, *Atmos. Chem. Phys.*, *9*, 515–527.

Hervig, M. E., L. L. Gordley, L. E. Deaver, D. E. Siskind, M. H. Stevens, J. M. Russell, S. M. Bailey, L. Megner, and C. G. Bardeen (2009), First satellite observations of meteoric smoke in the middle atmosphere, *Geophys. Res. Lett.*, *36*, L18805, doi:10.1029/2009GL039737.

Holton, J. R., P. H. Haynes, M. E. McIntyre, A. R. Douglass, R. B. Rood, and L. Pfister (1995), Stratosphere-troposphere exchange, *Rev. Geophys.*, *33*, 403–439.

Johnson, K. S. (2001), Iron supply and demand in the upper ocean: Is extraterrestrial dust a significant source of bioavailable iron?, *Global Biogeochem. Cycles*, *15*, 61–63.

Koide, M., and E. D. Goldberg (1977), Transuranic depositional history in South Greenland firn layers, *Nature*, *269*, 137–139.

Koide, M., R. Michel, E. D. Goldberg, M. M. Herron, and C. C. Langway Jr. (1979), Depositional history of artificial radionuclides in the Ross Ice Shelf, Antarctica, *Earth Planet. Sci. Lett.*, *44*, 205–223.

Krey, P. W. (1967), Atmospheric burnup of a plutonium-238 generator, *Science*, *158*, 769–771.

Krey, P. W., and B. Krajewski (1970), Comparison of atmospheric transport model calculations with observations of radioactive debris, *J. Geophys. Res.*, *75*, 2901–2908.

Lancelot, C., A. de Montety, H. Goosse, S. Becquevort, V. Schoemann, B. Pasquer, and M. Vancoppenolle (2009), Spatial distribution of the iron supply to phytoplankton in the Southern Ocean: A model study, *Biogeosciences*, *6*, 2861–2878.

Lanci, L., and D. V. Kent (2006), Meteoric smoke fallout revealed by superparamagnetism in Greenland ice, *Geophys. Res. Lett.*, *33*, L13308, doi:10.1029/2006GL026480.

Lanci, L., D. V. Kent, and P. E. Biscaye (2007), Meteoric smoke concentration in the Vostok ice core estimated from superparamagnetic relaxation and some consequences for estimates of Earth accretion rate, *Geophys. Res. Lett.*, *34*, L10803, doi:10.1029/2007GL029811.

Lanci, L., B. Delmonte, D. V. Kent, V. Maggi, P. E. Biscaye, and J. R. Petit (2012), Magnetization of polar ice: A measurement of terrestrial dust and extraterrestrial fallout, *Quat. Sci. Rev.*, *33*, 20–31.

Morgenstern, O., et al. (2010), Review of the formulation of present-generation stratospheric chemistry-climate models and associated external forcings, *J. Geophys. Res.*, *115*, D00M02, doi:10.1029/2009JD013728.

Pedro, J. B., J. R. McConnell, T. D. van Ommen, D. Fink, M. A. J. Curran, A. M. Smith, K. J. Simon, A. D. Moy, and S. B. Das (2012), Solar and climate influences on ice core Be-10 records from Antarctica and Greenland during the neutron monitor era, *Earth Planet. Sci. Lett.*, *355*, 174–186.

Plane, J. M. C. (2012), Cosmic dust in the Earth's atmosphere, *Chem. Soc. Rev.*, *41*, 6507–6518.

Saunders, R. W., and J. M. C. Plane (2011), A photo-chemical method for the production of olivine nanoparticles as cosmic dust analogues, *Icarus*, *212*, 373–382.

Saunders, R. W., S. Dhomse, W. S. Tian, M. P. Chipperfield, and J. M. C. Plane (2012), Interactions of meteoric smoke particles with sulphuric acid in the Earth's stratosphere, *Atmos. Chem. Phys.*, *12*, 4387–4398.

Smetacek, V., et al. (2012), Deep carbon export from a Southern Ocean iron-fertilized diatom bloom, *Nature*, *487*, 313–319.

Strahan, S. E., et al. (2011), Using transport diagnostics to understand chemistry climate model ozone simulations, *J. Geophys. Res.*, *116*, D17302, doi:10.1029/2010JD015360.

Tian, W., and M. P. Chipperfield (2005), A new coupled chemistry climate model for the stratosphere: The importance of coupling for future O_3 climate predictions, *Q. J. R. Meteorol. Soc.*, *131*, 281–303.